EBioMedicine 50 (2019) 81–92

Contents lists available at ScienceDirect

EBioMedicine

journal homepage: www.elsevier.com/locate/ebiom

Research paper

Celastrol-induced degradation of FANCD2 sensitizes pediatric high-grade gliomas to the DNA-crosslinking agent carboplatin

Dennis S. Metselaar[a,b], Michaël H. Meel[a,b], Bente Benedict[c], Piotr Waranecki[a,b], Jan Koster[d], Gertjan J.L. Kaspers[a,b], Esther Hulleman[a,b,*]

[a] Princess Máxima Center for Pediatric Oncology, Utrecht, the Netherlands
[b] Departments of Pediatric Oncology/Hematology, Emma Children's hospital, Amsterdam UMC, Vrije Universiteit Amsterdam, Cancer Center Amsterdam, Amsterdam, the Netherlands
[c] Division of Tumor Biology and Immunology, the Netherlands Cancer Institute, Amsterdam, the Netherlands
[d] Department of Oncogenomics, Amsterdam UMC, University of Amsterdam, Amsterdam, the Netherlands

ARTICLE INFO

Article History:
Received 31 July 2019
Revised 26 October 2019
Accepted 31 October 2019
Available online 14 November 2019

Keywords:
Pediatric high-grade glioma
Preclinical therapy development
FANCD2
DNA-crosslinking
Celastrol

ABSTRACT

Background: Pediatric high-grade gliomas (pHGG) are the leading cause of cancer-related death during childhood. Due to their diffuse growth characteristics, chemoresistance and location behind the blood-brain barrier (BBB), the prognosis of pHGG has barely improved in the past decades. As such, there is a dire need for new therapies that circumvent those difficulties. Since aberrant expression of DNA damage-response associated Fanconi anemia proteins play a central role in the onset and therapy resistance of many cancers, we here investigated if FANCD2 depletion could sensitize pHGG to additional DNA damage.
Methods: We determined the capacity of celastrol, a BBB-penetrable compound that degrades FANCD2, to sensitize glioma cells to the archetypical DNA-crosslinking agent carboplatin *in vitro* in seven patient-derived pHGG models. In addition, we tested this drug combination *in vivo* in a patient-derived orthotopic pHGG xenograft model. Underlying mechanisms to drug response were investigated using mRNA expression profiling, western blotting, immunofluorescence, FANCD2 knockdown and DNA fiber assays.
Findings: FANCD2 is overexpressed in HGGs and depletion of FANCD2 by celastrol synergises with carboplatin to induce cytotoxicity. Combination therapy prolongs survival of pHGG-bearing mice over monotherapy and control groups *in vivo* ($P<0.05$). In addition, our results suggest that celastrol treatment stalls ongoing replication forks, causing sensitivity to DNA-crosslinking in FANCD2-dependent glioma cells.
Interpretation: Our results show that depletion of FANCD2 acts as a chemo-sensitizing strategy in pHGG. Combination therapy using celastrol and carboplatin might serve as a clinically relevant strategy for the treatment of pHGG.
Funding: This study was funded by a grant from the Children Cancer-Free Foundation (KIKA, project 210). The disclosed funders had no role in study design, data collection and analysis, decision to publish, or preparation of the manuscript.
© 2019 The Authors. Published by Elsevier B.V. This is an open access article under the CC BY-NC-ND license. (http://creativecommons.org/licenses/by-nc-nd/4.0/)

Research in context

Evidence before this study

Pediatric high-grade gliomas (HGG) are highly malignant brain tumors with a devastating prognosis, contributing to the most cancer related mortalities in children. Expression of FANCD2, a member of the Fanconi anemia group genes, known to be involved in DNA repair, has been linked to glioma grade in adults. In addition, inhibition of FANCD2 has been shown to induce cisplatin sensitivity in lung cancer models *in vitro*. Celastrol is a natural compound that has been shown to degrade FANCD2 via activation of the proteasome. Several studies propose celastrol as a suitable compound against Alzheimers disease progression, by highlighting its neuroprotective properties and ability to cross the blood-brain barrier, which contributes to the translational potential of celastrol in brain tumor studies.

Added value of this study

Our study identifies FANCD2 as a therapeutic target in pediatric HGG. We developed a synergistic treatment strategy that

* Corresponding author: Princess Máxima Center for Pediatric Oncology, Heidelberglaan 25, 3584CS Utrecht, the Netherlands.
E-mail address: e.hulleman@prinsesmaximacentrum.nl (E. Hulleman).

https://doi.org/10.1016/j.ebiom.2019.10.062
2352-3964/© 2019 The Authors. Published by Elsevier B.V. This is an open access article under the CC BY-NC-ND license. (http://creativecommons.org/licenses/by-nc-nd/4.0/)

uses the brain bioavailable FANCD2 inhibitor celastrol to sensitize pHGG to the classical chemotherapeutic carboplatin. A genetically diverse panel of primary patient-derived pHGG cultures all showed a synergistic antitumor response to this drug combination. Moreover, survival of mice carrying primary patient-derived pHGG xenografts was significantly prolonged by combined treatment with celastrol and carboplatin. Altogether, these findings may lead to the development of a multimodal therapeutic strategy for pHGG based on FANCD2 inhibition.

Implications of all the available evidence

This study shows an effective treatment in pediatric high-grade gliomas *in vitro* and *in vivo*. However, as FANCD2 overexpression is also detected in adult high-grade gliomas, this treatment strategy might be extrapolated to this patient group as well. However, since pure celastrol may have a narrow therapeutic window, ideally alternative FANCD2 inhibitors or synthetic celastrol analogues should be used for clinical translation. Furthermore, future studies should investigate if other classes of DNA damaging agents can be more effective in co-treatment with celastrol.

1. Introduction

Pediatric high-grade gliomas (pHGG) are among the most lethal malignancies in children. Despite recent advances in understanding the molecular basis of these tumors, clinical prognosis for pHGG patients has not yet improved. pHGG are characterised by epigenetic modifications and defects in DNA damage repair genes. However, little is known about non-mutated DNA-damage repair genes that are deregulated in pHGG.

Disruption of the Fanconi DNA-repair mechanism has been linked to the onset of several malignancies through a syndrome called Fanconi anemia (FA), a genetic disorder caused by germline mutations in any of the genes coding for one of the Fanconi proteins [1–3]. FA is associated with genomic instability and strong sensitivity to DNA-crosslinking analogues, because of the absence of an operational Fanconi machinery [4]. Fanconi anemia group D2 (FANCD2), one of the core components of the Fanconi repair mechanism, induces an intracellular response to DNA damage upon complexing with FANCI [5]. In contrast to cancers harbouring mutated Fanconi components, little is known about cancers with deregulated, yet non-mutated, Fanconi core components.

In this study we show that FANCD2 expression levels increase with glioma grade, as is supported by earlier findings [6]. We hypothesised that HGGs are highly dependent on the Fanconi system for DNA repair and that disruption of this mechanism would make these tumors prone to DNA-crosslinking agents, as seen in FA patients [4].

To study if depletion of the deregulated FANCD2 in pHGG cells could cause a FA-like phenotype that leads to a higher sensitivity to platina analogues, we treated primary pHGG cells with carboplatin in combination with celastrol, a blood-brain barrier (BBB) permeable compound that has been shown to cause degradation of FANCD2 via the proteasome [7,8]. In our experiments, carboplatin was chosen over other platinum chemotherapeutics because of its relatively mild neurotoxic side effects and reported ability to cross the BBB [9,10].

Here we show that depletion of FANCD2 by celastrol treatment provokes stalled fork replication and causes sensitivity to the DNA-crosslinking agent carboplatin in primary pHGG cells. Furthermore we show that treatment of mice carrying primary patient-derived pHGG xenografts with this combination of drugs leads to prolonged survival, as compared to monotherapy.

2. Materials and methods

2.1. Cell cultures

HSJD-DIPG-07 [11] (H3.3K27M, DIPG) was a kind gift from Dr Montero Carcaboso (Hospital San Joan de Déu, Barcelona, Spain), JHH-DIPG-01 [12] (H3.3K27M, DIPG) from Dr Raabe (John Hopkins Hospital, Baltimore, USA), and SU-DIPG-IV (H3.1K27M, DIPG) and SU-pcGBM2 (H3 wildtype, GBM) [13] from Dr Monje (Stanford University, Stanford, USA). VUMC-DIPG-10 [14] cells were established at the VU University Medical Center from a DIPG autopsy (H3 wildtype), while VUMC-DIPG-F [15] and VUMC-DIPG-G are biopsy-derived H3.3K27M DIPG cultures. VUMC-HGG-05 [16] (giant-cell GBM), VUMC-HGG-09 (IDH1 R132H) and VUMC-HGG-14 are resection-derived glioblastomas. VUMC-HGG-11 [17] is a thalamic midline glioma harbouring a H3.3 K27M mutation. All models are FANCD2 wild-type as confirmed by whole-genome sequencing.

Cells were cultured as neurospheres as previously described [15,17,18]. Cells were only used when confirmed mycoplasm negative and short-tandem repeat (STR) analysis was performed to ensure cell line identities.

2.2. Human mRNA expression datasets

The following expression datasets were used to study mRNA expression between patients:

Healthy brain (GSE 11882 and 13564) [19,20], healthy cerebellum (GSE 3526) [21], glioma (GSE 16011 and 4290) [22,23], glioblastoma (GSE 7696) [24], pediatric HGG (GSE 19578) [25], pediatric DIPG (GSE 26576) [26]. Survival correlation to FANCD2 expression was studied using the glioma dataset GSE 43378 [27].

2.3. Chemicals

Celastrol (CAS № 34157-83-0), carboplatin (CAS № 41575-94-4), MG-132 (CAS № 133407-82-6), and topotecan (CAS № 123948-87-8) were purchased from Cayman Chemical Company (Ann Arbor, Michigan, USA). For *in vitro* studies, celastrol, topotecan and MG-132 were dissolved in DMSO and stored at a 10 mM concentration. Carboplatin was stored as a 10 mM stock dissolved in H_2O for increased stability compared to storage in DMSO [28]. For *in vivo* studies, celastrol was dissolved in DMSO, and carboplatin was dissolved in 0.9% saline.

2.4. Cell viability assays

For cell viability assays, cells were plated at a density of 5000 cells/well in 96-well F-bottom cell-repellent plates (Greiner Bio-one, #650971). 24 h after cell seeding, drugs were dispensed at different concentrations using a Tecan D300e picoliter dispenser (Tecan Group Ltd, Switzerland) and incubated at 37 °C and 5% CO_2 for 96 h. CellTiter-Glo® 3D Luminescent Cell Viability Assay (Promega) was used as a method to determine the number of viable cells in culture following manufacturer's protocol. Luminescence was measured using a Tecan Infinite® 200 reader using iControl 1.10 software. Synergy scores are based on average cell viability at 96 h after treatment at the indicated concentrations and were calculated using the Synergyfinder software.

2.5. Western blotting

Immunoblotting was performed as previously described [15]. Protein was isolated using RIPA lysis buffer supplemented with protease and phosphatase inhibitors. Membranes were incubated with Rabbit anti-FANCD2 (1:1000, Abcam, Cambridge, UK, #ab108928), mouse anti-phospho-Histone H2A.X (Ser139) (1:2000, Millipore, Burlington, MA, USA, #05-636), rabbit anti-RAD51 (D4B10) (1:1000, Cell

Signaling Technology, #8875 s), or mouse anti-Actin (MAB1501) (1:10,000, Millipore, #3018,859). Subsequently, membranes were incubated with secondary goat anti-rabbit IRDye© 800CV antibody (1:20,000, LI-COR©, Lincoln, NA, USA) and/or goat anti-mouse IRDye© 600CV antibody (1:10,000, LI-COR©). Signal detection was performed using a LI-COR© Oddyssey fluorescent imager (model 9120; Surplus Solutions, LLC).

2.6. RNA sequencing

JHH-DIPG-01, HSJD-DIPG-07, SU-pcGBM2, and SU-DIPG-IV neurospheres were treated with 100 nM celastrol, 1 μM carboplatin, or a combination thereof. After 24 h, cells were collected and RNA was extracted using the miRvana miRNA isolation kit without phenol (Ambion, Life Technologies, NL), supplemented with Acid-Phenol: Chloroform. Subsequently, RNA-quality was analyzed with the Agilent 2100 Bioanalyzer using the Agilent RNA 6000 Nano Kit (Thermo Fisher, Waltham). Only samples that received a RIN>7 were further processed.

Sequencing was performed using an Illumina Nextseq 500 sequencer according to the manufacturer's instructions. Alignment, feature counts, and differential expression were analyzed using the RNA-Seq v5 pipeline (GenomeScan, Leiden, NL). The human Ensembl GRCh37.75 reference was used for alignment of the reads for each sample. The reads were mapped to the reference sequence using a short read aligner based on Burrows-Wheeler Transform (Tophat v2.0.14) with default settings. The read counts were loaded into the DESeq2 package v1.14.1 within the R platform v3.3.0 for statistical analysis. Fastq files were uploaded to the R2 platform (r2.amc.nl) for further analysis and statistics. A list of all differentially expressed genes between the non-treated and celastrol treated groups is added as supplementary file 1.

2.7. Immunofluorescent imaging

VUMC-HGG-09 cells were cultured in TSM supplemented with FCS in Greiner SCREENSTAR® 96-well plates (#655-866) specialised for fluorescent imaging. Cells were treated with celastrol, carboplatin or a combination thereof for 12 h. Hereafter, cells were washed with ice cold PBS and fixed in 4% paraformaldehyde. After blocking (PBS + 1% BSA for 30 min) and permeabilisation (PBS +0,1% triton-X for 30 min), primary antibodies, rabbit anti-FANCD2 (1:1000, Abcam, #ab108928), and mouse Anti-phospho-Histone H2A.X (Ser139) (1:2000, Millipore, #05-636), were added to the slides for overnight incubation at 4 °C. As secondary step Alexa Fluor™ 488 (goat anti-rabbit, 1:10,000, Invitrogen, #411-667) and Alexa Fluor™ 594 (goat anti-mouse, 1:10,000, Invitrogen, #1887003) were incubated for 1 h at RT. Imaging was done using the Zeiss AxioObserver Z1 inverted microscope using a 40x and 63x objective equipped with a Hamamatsu ORCA AG Black and White CCD camera. Quantification of yH2AX foci was done using ImageJ software, according to the automatic particle analysis for cell counting (200px^2), followed by automatic single point selection overlay (noise tolerance 45).

2.8. Neutral comet assay

To detect DNA double-strand breaks (DSBs), neutral comet assays were performed as previously described [29]. Shortly, cells were harvested, 8000 cells were diluted in 400 μl PBS and embedded in 1.2 ml 1% low-gelling agarose (Sigma). 100 μl of the cell suspension was used to make gels onto Trevigen comet assay slides. To lyse the cells in the gel, slides were incubated in lysis solution (2% sarkosyl, 0.5 M Na_2EDTA and 0.5 mg/ml Proteinase K) overnight at 37 °C. The next day, slides were rinsed three times for 30 min at room temperature in electrophoresis buffer (90 mM TrisHCl pH = 8.5, 90 mM Boric Acid and 2 mM Na_2EDTA). Electrophoresis was performed for 25 min at 20 V in electrophoresis buffer. Subsequently, slides were washed once with distilled water. To stain DNA slides were incubated with 2.5 μg/ml Propidium Iodide diluted in distilled water for 20 min. Individual comets were imaged with a Zeiss AxioObserver Z1 inverted microscope using a 20x objective equipped with a Hamamatsu ORCA AG Black and White CCD camera. Tailmoments of individual comets were assessed using the CASP software (http://casplab.com/). For each condition, more than 50 cells were analyzed.

2.9. DNA fiber assay

DNA fiber assays were performed as previously described [30]. Briefly, cells were pulse labelled with 25 μM CldU followed by 250 μM IdU for 30 min each. Labelled cells were trypsinised, lysed in spreading buffer (200 mM Tris-Hcl pH7.4, 50 mM EDTA and 0.5% SDS) and spread on microscope slides (Menzel-Gläser, Superfrost). DNA fibers were fixed on slides using 3:1 methanol: acetic acid. Slides were treated with 2.5 M HCl for 1 h and 15 min to denature DNA followed by 1 h incubation in blocking buffer (PBS, 1% BSA, 0.1% Tween20). For detection of CldU and IdU, slides were incubated for 1 h with rat-anti-Brdu (Clone BU1/75, Abcam; 1:500) and mouse-anti-BrdU (clone B44, Becton Dickinson; 1:750), respectively. Subsequently, slides were fixed with 4% paraformaldehyde for 10 min and incubated with Alexa 488-labeled goat-anti-mouse and Alexa 555-labeled goat-anti-rat (Molecular probes; 1:500) for 1.5 h. DNA fibers were imaged with the Zeiss AxioObserver Z1 inverted microscope using a 63x objective equipped with a Hamamatsu ORCA AG Black and White CCD camera. Replication track lengths were analyzed using ImageJ software and the conversion factor 1 μm = 2.59 kb was used [31].

2.10. Establishment of stable FANCD2 knockdown cells

FANCD2 knockdown cells were established using the pLKO.1-shFANCD2.1 and pLKO.1-shFANCD2.2 (GE Healthcare, Chicago, USA) plasmids as described previously [17]. shRNA sequences are summarised in supplementary table S1.

2.11. In vivo experiments

4-week old female athymic nude mice (FVB foxn1$^{-/-}$) were purchased from Charles River Laboratories ('s-Hertogenbosch, NL) and housed in compliance with European and national guidelines for experimental animal research (protocol #841-NCH17-04, animal welfare committee, Vrije Universiteit, Amsterdam). After one week of acclimatisation, VUMC-HGG-14 cells (50*10^4 cells in 5μL) were stereotactically injected into the striatum (bregma:x-2 mm;y0.5 mm;z-3 mm), and tumor growth was followed longitudinally by bioluminescence imaging (BLI) using the IVIS Spectrum (Perkin Elmer, Waltham, MA, USA). When tumor growth showed a stably increasing signal in all animals, mice were stratified into four groups based on absolute BLI signal and signal increase between last two measurements. Group A received saline (0.9%) intravenously (I.V.) and water via oral gavage (O.G.). Group B received carboplatin (150 mg/kg) once a week via I.V. injection [32] and water orally. Group C received celastrol (2.5 mg/kg) via O.G. [33] daily for five consecutive days, and after one week off-treatment a second five day treatment round, this time of 5 mg/kg celastrol per day. Group C received 0.9% saline via I.V. injection. Group D was treated with both celastrol and carboplatin as described for group B and C. Survival was scored based on humane endpoints, which were defined as *a* >20% loss of body mass from highest weight or severe neurological deficits. Only mice that experienced tumor metastasis into the ventricles within two weeks after injection were excluded from the study, as these were considered implantation errors.

Table 1
Overview of the pediatric high-grade glioma models used in this study.

Model	Age	Location	Diagnosis	H3 mutation	Other mut.	Treatment
VUMC-DIPG-F	7y, ♂	Pons	DIPG	H3.3K27M		Biopsy (no treatment)
VUMC-DIPG-G	*, ♀	Pons	DIPG	H3.3K27M	*TP53*	Biopsy (no treatment)
VUMC-HGG-05	11y, ♀	Cortical	GBM	WT	*TP53*	Resection (no treatment)
VUMC-HGG-09	11y, ♀	Cortical	GBM	WT	*IDH1 TP53*	Biopsy/resection (no treatment)
VUMC-DIPG-10	12y, ♀	Pons	DIPG	WT	*NF-1*	Autopsy, XRT+gemcitabine
VUMC-HGG-11	*, ♀	Thalamus	Thalamic glioma	H3.3K27M	*TP53*	Biopsy/resection (no treatment)
VUMC-HGG-14	17y, ♂	Cortical	GBM	WT	*BRAF*	Biopsy/resection (no treatment)
HSJD-DIPG-07	6y, ♂	Pons	DIPG	H3.3K27M	*ACVR1*	Autopsy (no treatment)
JHH-DIPG-01	8y, ♂	Pons	DIPG	H3.3K27M	*TP53*	Autopsy, XRT+carboplatin/etoposide, sorafenib/erlotinib, irinotecan/temozolomide, irinotecan/bevacizumab
SU-DIPG-IV	2y, ♀	Pons	DIPG	H3.1K27M	*ACVR1, TP53*	Autopsy, XRT+cetuximab/irinotecan
SU-pcGBM2	15y, ♂	Cortical	GBM	WT	*NF-1, TP53*	Diagnosis sample (no treatment)

* = *Age unknown*.

Upon reaching their humane endpoint, mice were euthanised by Euthasol® 20% (AST Farma, Oudewater, NL), after which brains were collected and fixed in 4% paraformaldehyde for 48 h. The fixed brains were embedded in paraffin and processed for human-vimentin immunohistochemical staining (mouse-anti-human-vimentin, clone V9, #M0725, DAKO, Santa Clara, USA). Human-vimentin stainings were imaged using the Vectra® Polaris™ Automated Quantitive Pathology Imaging System (Perkin Elmer, Waltham, USA). Furthermore, the brains were processed for KI-67 and cleaved caspase-3 immunohistochemical stainings (rabbit-anti-KI-67, clone D2H10, #9027S and rabbit-anti-cleaved caspase 3, clone ASP175, #9661S, both from Cell Signaling Technology). KI-67 and cleaved caspase-3 stainings were imaged using a Zeiss Axio optical microscope equiped with a Zeiss Axiocam ICc5 operated by ZEN Pro-imaging software. All brains used for these stainings originate from mice that were euthanised approximately three weeks after finishing the full treatment protocol.

2.12. Statistics

mRNA expression between groups from RNA-sequencing data was assessed using the one-way analysis of variance (ANOVA). *In vitro* cell survival percentages were compared using the independent *t*-test (two-sided). drug synergy was calculated using the Synergyfinder software [34], which uses the Zero interaction potency (ZIP) model to create synergy scores [35]. DNA-fiber assay and comet assay groups were compared using the Mann–Whitney *U* test. *In vivo* survival differences between groups were tested using the log-rank (Mantel-Cox) test. The statistical analyzes were performed using Microsoft Excel (Microsoft Office 2010) and GraphPad Prism (version 6). A p-value <0.05 was considered statistically significant.

3. Results

3.1. FANCD2 is overexpressed in pediatric high-grade gliomas

To evaluate if expression of Fanconi complex genes correlates with glioma-grade, we analyzed mRNA expression of Fanconi genes in publicly available gene expression datasets. Therefore, we used the R2 platform (r2.amc.nl), a database that includes gene expression profiles from large patient cohorts, including tools to compare gene expression between different cancer types. We found that the expression of *FANCD2* in HGG tumor tissues is upregulated compared to healthy brain tissues (172 healthy brain tissues and 9 healthy cerebellum tissues compared to 368 adult HGG and 90 pediatric HGG tumor samples), as depicted in Fig. 1a. On average, tumor tissue showed a 12-fold upregulation of *FANCD2* compared to healthy brain ($P < 0.0001$ for all glioma samples *vs*. healthy brain and cerebellum). Also, *FANCD2* mRNA expression levels significantly correlated with glioma grade (Fig. 1b), as did patient survival (Fig. 1c). Furthermore, we found markedly less overexpression of other genes of the Fanconi complex in HGGs compared to healthy brain tissue (Supplementary figure S1), suggesting that in HGGs FANCD2 plays an additional role independently of the classical Fanconi complex mechanism.

To validate the patient cohort finding, we assessed FANCD2 protein expression profiles in a panel of pHGG cells by western blotting (Fig. 1d), using FANCD2 protein expression in human astrocytes as a healthy control. All pHGG models showed expression of FANCD2, albeit with different expression levels, while human astrocytes showed no visible FANCD2 protein expression. An overview, including details on the molecular background and treatment history, of all the pHGG models used in this study is depicted in Table 1.

3.2. FANCD2 is degraded upon celastrol treatment in primary pHGG cells

To test the effect of FANCD2 downregulation in our pHGG cell cultures, we used the plant derivate celastrol, which has been reported to induce degradation of FANCD2 via proteasome activity [8]. Therefore, we treated three different pHGG cultures with celastrol for 24 h and observed a strong decrease in FANCD2 protein expression in all models (Fig. 2a). We then compared RNA-sequencing results of four treated pHGG models (HSJD-DIPG-07, JHH-DIPG-01, SU-DIPG-IV, SU-pcGBM2) to their non-treated controls through a parametric analysis of gene set enrichment (PAGE), using the KEGG database. This analysis showed a significant differential expression of the proteasome geneset between the non-treated and celastrol-treated groups (FDR-corrected, $P<0.05$) (Fig. 2b), suggesting that celastrol treatment alters proteasome activity in our pHGG cultures. Furthermore, comparison between the non-treated and celastrol-treated groups revealed no difference in FANCD2 mRNA expression ($P = 0.41$), suggesting that celastrol alters FANCD2 expression in a post-transcriptional manner (Supplementary figure S2). These results were further confirmed by treating two pHGG cultures with the proteasome inhibitor 'MG-132′ [36], followed by celastrol treatment, which rescued FANCD2 protein expression (Fig. 2c). Together, these results imply proteasomal degradation as a mechanism that degrades FANCD2 in pHGG cells after celastrol treatment.

3.3. Celastrol and carboplatin produce synergistic cytotoxicity in primary pHGG cells

Because FANCD2 overexpression in pHGG suggested a Fanconi repair pathway dependency, we hypothesised that celastrol-driven FANCD2 degradation could sensitize pHGG cells to DNA-crosslinking

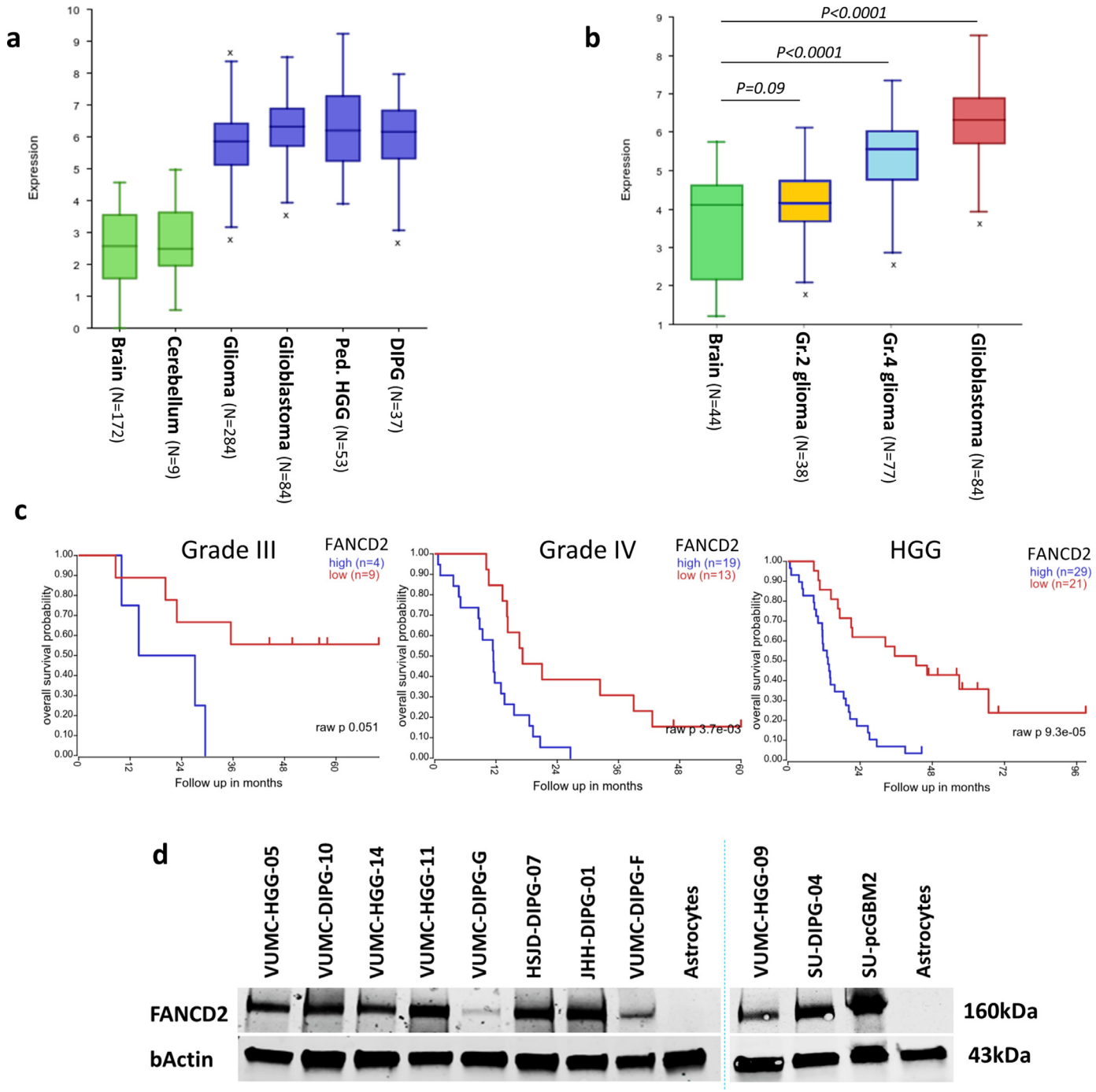

Fig. 1. FANCD2 is overexpressed in high-grade gliomas.

(a) FANCD2 mRNA expression levels in healthy brain and healthy cerebellum tissues (green), compared to high-grade glioma; both adult and pediatric (blue) (GSE ID in order: 11882 [19], 3526 [21], 16011 [22], 7696 [24], 19578 [25], 26576 [26]). $P < 0.0001$ for any glioma dataset *vs*. normal brain and cerebellum (one-way ANOVA)

(b) mRNA expression levels of FANCD2 in normal brain (green, GSE13564 [20]), compared to gliomas of different grades: grade 2 (yellow, GSE4290 [23]), grade 3 (blue, GSE4290 [23]), grade 4 GBM (red, GSE7696 [24]).

P-values were determined by one-way ANOVA between datasets.

(c) Kaplan-Meijer curves representing survival of grade 3 HGG patients (left), grade 4 HGG patients (middle), and grade 3 and 4 HGG overall (right) as determined using the publicly available R2 platform. Red lines represent low-FANCD2 mRNA tumor expression *vs*. high-FANCD2 mRNA expression in blue (GSE43378 [27], expression cutoff: 68.8).

Note: In Fig. 1a, b, and c no individual samples were excluded.

(d) Western blots showing baseline expression levels of FANCD2 in a panel of primary pHGG cultures. Human astrocytes were used as control sample; actin was used as a loading control

Figs. a, b and c were generated using the R2 platform (HYPERLINK "http://r2.amc.nl"). (For interpretation of the references to color in this figure legend, the reader is referred to the web version of this article.)

agents. Therefore, we investigated the effect of celastrol and carboplatin monotherapy and a combination of both compounds on a panel of primary pHGG cell cultures. Cells were treated for 96 h with both compounds at a range of concentrations to determine cytotoxic IC50. Celastrol IC50 concentrations ranged from 0.5 μM to 3 μM (Fig. 3a, c), while carboplatin IC50 concentrations ranged between 10 and 24 μM (Fig. 3b, c). Importantly, combination treatment caused synergistically increased cytotoxicity, especially when semi-toxic

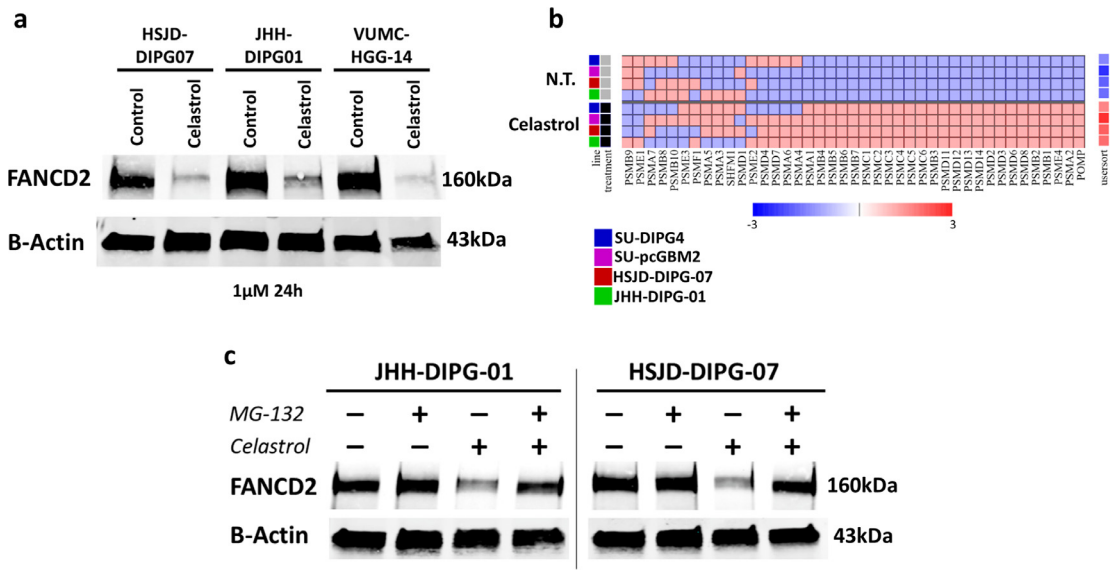

Fig. 2. Celastrol degrades FANCD2 partly via the proteasome.

(a) Western blot analysis showing depletion of FANCD2 after celastrol (1 μM) treatment for 24 h.

(b) Heatmap representation illustrating mRNA expression of the KEGG proteasomal geneset from RNA-sequencing data showing four non-treated (N.T.) *versus* celastrol-treated pHGG cultures (HSJD-DIPG-07, JHH-DIPG-01, SU-DIPG-IV, SU-pcGBM2) (PAGE FDR $P < 0.05$).

(c) Western blot analysis showing rescue of FANCD2 protein depletion after proteasome inhibition using MG-132 (10 μM) for 2 h, followed by celastrol (1 μM) for 6 h.

(IC-50) celastrol concentrations were combined with nontoxic carboplatin concentrations (Fig. 3d, e). Similar experiments with topotecan, an effective DNA-damaging topoisomerase inhibitor often used to treat GBM, instead of carboplatin in three pHGG cell lines (VUMC-HGG-05, JHH-DIPG-01, and HSJD-DIPG-07) showed no synergistic effect on cell viability (Supplementary Figure S3) [37].

FANCD2 knockdown by shRNA in pHGG cultures resulted in a similar sensitisation to carboplatin cytotoxicity as celastrol treatment, confirming the FANCD2-dependence of the observed synergy (Fig. 4a-b). As expected, celastrol monotherapy sensitivity was not effected in all FANCD2 shRNA pHGG cultures, suggesting the need for a trigger, like carboplatin, to take advantage of the absent repair machinery (Supplementary figure S4).

3.4. Celastrol induces genomic instability by arresting the replication fork

To determine whether the synergistic effect of celastrol was related to the DNA-damaging effect of carboplatin, we examined the expression of γH2AX by immunofluorescence after treatment with either compound as monotherapy, or in combination [38]. While celastrol monotherapy depleted FANCD2 expression, no accumulation of the DNA-damage marker γH2AX was observed. Treatment of VUMC-HGG-09 cells with carboplatin, however, caused nuclear accumulation of γH2AX (Fig. 5a, b, c). The number of foci increased when carboplatin treatment was combined with celastrol, leading to a further accumulation of γH2AX foci within the nucleus. Similar results were obtained for different pHGG cultures by western blotting, although in some cases an increase in γH2AX expression was observed upon celastrol monotherapy as well (Fig. 5d).

To confirm that the γH2AX accretion after celastrol and carboplatin combination therapy was the result of accumulation of double strand breaks (DSBs), we made use of the neutral comet assay that determines the length of DNA tails as a measure for DSBs [29]. Unexpectedly, in both the JHH-DIPG-01 and HSJD-DIPG-07 a significant ($P<0.0001$) increase in tail length was observed after celastrol treatment, while carboplatin treatment did not induce an increased amount of DSBs (Fig. 5e, f). Combination therapy induced a similar average tail length as the celastrol treated group, suggesting that celastrol is solely responsible for DSB accumulation after 24 h of treatment, which is paradoxical with our γH2AX measurements. However, other mechanisms may account for the differential accumulation of γH2AX foci between celastrol mono- and combination treatment, such as stability of the replication fork. Recent literature suggests a direct connection between FANCD2 expression and replication fork stability via RAD51 and SETD1A [39,40]. Therefore, we assessed the expression of these proteins before and after celastrol treatment by western blot. As shown in Fig. 5g-h, both RAD51 and SETD1A protein expression decreased after 24 h of celastrol treatment. Like the results in the cell-viability assays, downregulation of RAD51 upon celastrol treatment appears to depend on the presence of FANCD2, as stable knockdown of FANCD2 decreases protein levels of RAD51 as well (Fig. 5e).

To further confirm that celastrol caused stalled replication forks via depletion of FANCD2, we used a DNA fiber assay to analyze the DNA synthesis rate. After treating pHGG cells for 24 h with celastrol we found a significant ($P<0.0001$) decrease in replication fork progression in all cultures compared to controls (Fig. 5i), indicating that celastrol arrests the replication fork.

3.5. Celastrol and carboplatin combination treatment prolongs survival in a pHGG xenograft model

To determine the therapeutic efficacy of celastrol and carboplatin *in vivo*, we tested these compounds in athymic nude mice carrying patient-derived pediatric glioblastoma xenografts (VUMC-HGG-14). This model was established from surgical resection material of a GBM from a pediatric patient and shows a typical GBM-like growth pattern in the mice (Fig. 6a). VUMC-HGG-14 cells were transduced *in vitro* with luciferase in order to monitor intracranial tumor-burden *in vivo* in time and were validated using STR analysis. Treatment started 15 days after tumor implantation upon demonstration of engraftment by bioluminescence imaging (BLI), at which moment mice were stratified into four equivalent groups (control, carboplatin (150 mg/kg), celastrol (2.5 and 5 mg/kg), and combination) based on BLI signal intensity [41]. Since no toxicity was observed after the first treatment round, we increased the

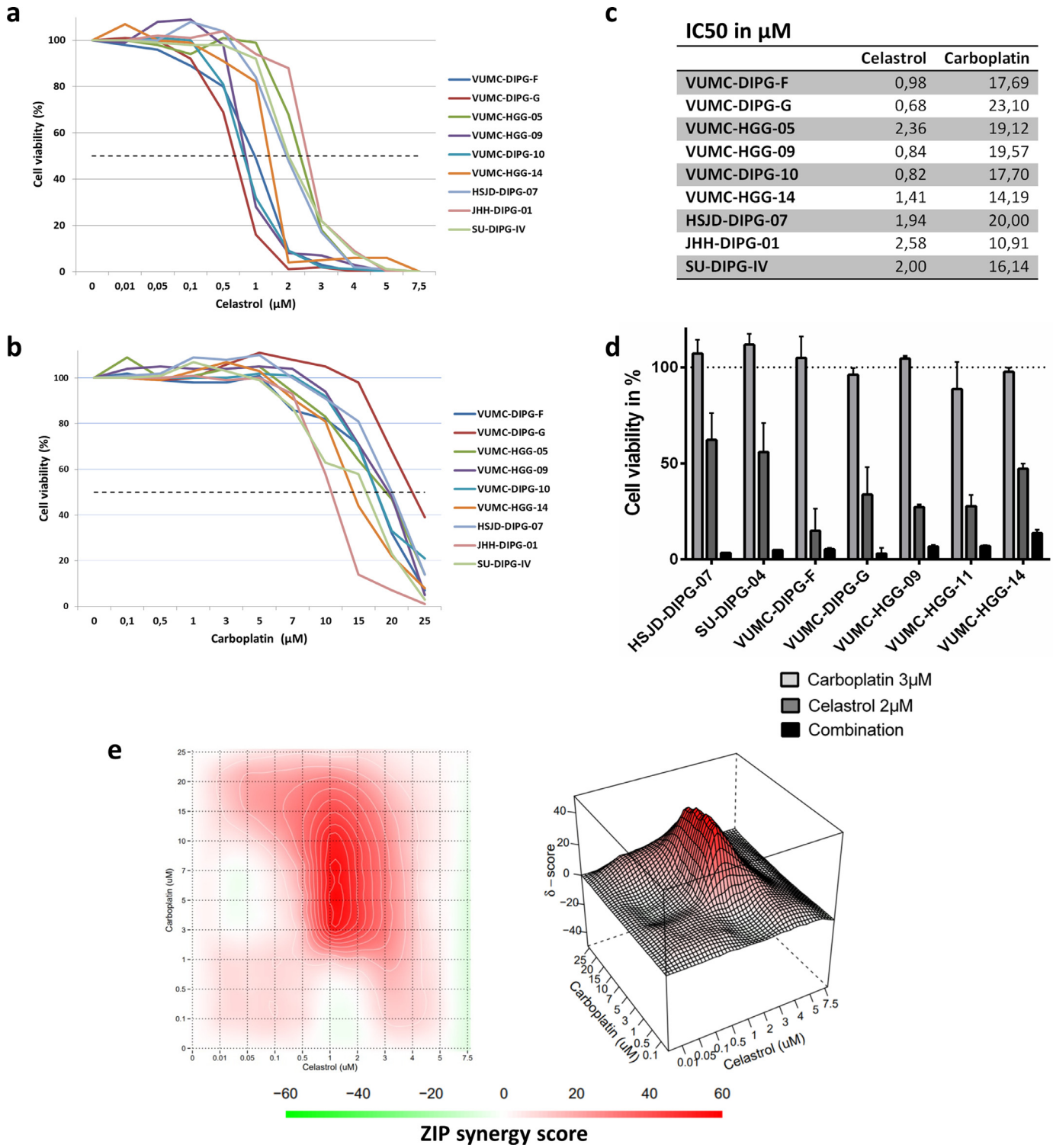

IC50 in µM

	Celastrol	Carboplatin
VUMC-DIPG-F	0,98	17,69
VUMC-DIPG-G	0,68	23,10
VUMC-HGG-05	2,36	19,12
VUMC-HGG-09	0,84	19,57
VUMC-DIPG-10	0,82	17,70
VUMC-HGG-14	1,41	14,19
HSJD-DIPG-07	1,94	20,00
JHH-DIPG-01	2,58	10,91
SU-DIPG-IV	2,00	16,14

Fig. 3. Celastrol sensitizes pHGG cells to carboplatin *in vitro*

(a) Dose-response curves representing cell viability of primary pHGG models after celastrol treatment for 96 h.

(b) Dose-response curves representing cell viability of primary pHGG models after carboplatin treatment for 96 h.

(c) IC50 values (in μM) for each cell line to celastrol and carboplatin mono therapy.

(d) Bar graph visualizing relative cell viability of seven primary pHGG models at 96 h of treatment with either 3 μM carboplatin, 2 μM celastrol, or the combination thereof. The combination treatments show a synergistic effect on cell viability compared to the monotherapies. Error bars represent +/− SEM ($n = 6$). Cell viability is relative to DMSO-treated controls.

(e) 2D (left) and 3D (right) visualization of average synergy between celastrol and carboplatin at various concentrations in the seven pHGG cell models used in Fig. 3c. ZIP synergy scores >0 indicate synergism (in red). Maximum calculated synergy score = 48,35 (scores >10 are considered highly synergistic).

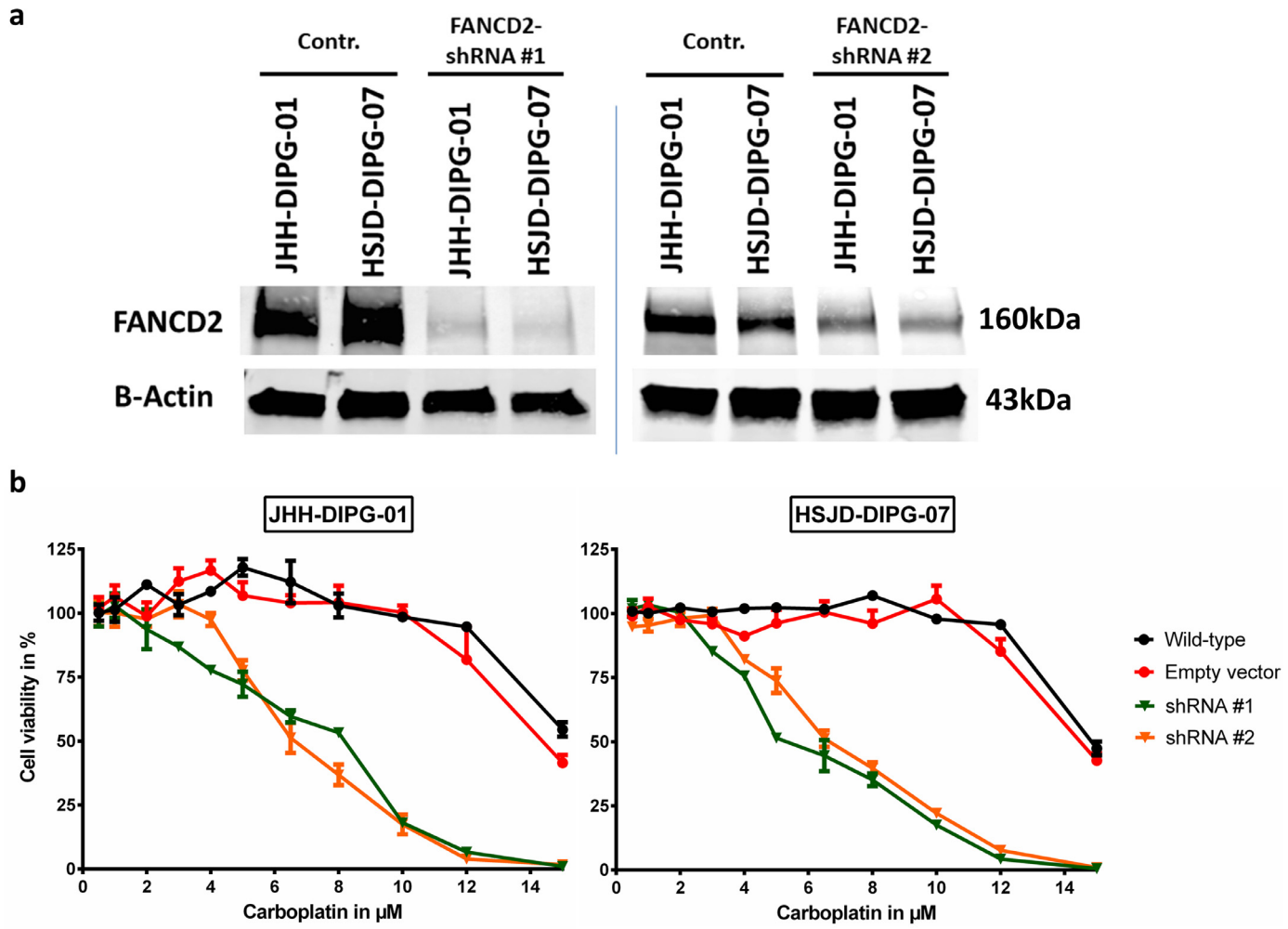

Fig. 4. FANCD2 knockdown induces carboplatin sensitivity.

(a) Western blot analysis showing FANCD2 expression in shRNA-control and FANCD2-shRNA expressing pHGG cells.

(b) Dose-response curves illustrating the cytotoxic effect of carboplatin monotherapy in two different wild-type, empty-vector, and two FANCD2-shRNA expressing pHGG cell models. Cell viability in the FANCD2 knockdown cells is depicted in green (shRNA#1) and orange (shRNA#2) *vs*. wildtype cells depicted in black and shRNA-control cells in red. (For interpretation of the references to color in this figure legend, the reader is referred to the web version of this article.)

celastrol dose from 2.5 mg/kg to 5 mg/kg in the second round. No treatment-related toxicities were observed and all mice developed GBM. Using 20% weight loss or the development of severe neurological deficits as humane endpoints, we observed a significantly increased survival of the celastrol/carboplatin combination therapy group compared to the control or monotherapy groups (median survival increase of 43% *versus* control; $P<0.05$ for combination *vs* any other group (log-rank test), Fig. 6b). In the combination treatment group we observed a trend towards less neurological deficits, as based on dropout causes per group (Supplementary Figure S5a). Furthermore, we observed normal weight distributions between groups and found no trend in longitudinal BLI signals (Supplementary Figure S5b-c). tumor propagation after treatment was investigated by immunostaining the proliferation marker Ki-67. Expression of Ki-67 was decreased upon celastrol and carboplatin combination therapy, while no difference was observed in Ki-67 expression between tumors treated with monotherapy and controls (Fig. 6c). Furthermore, immunostaining of cleaved caspase-3 as a marker of apoptosis showed no difference between the four groups in both malignant and non-malignant brain areas (Supplementary Figure S6).

4. Discussion

In this study we found that FANCD2 serves as a guardian against carboplatin induced toxicity in pHGG. We used the natural compound celastrol to induce degradation of FANCD2 in pHGG cells and show that this creates a therapeutic window for the platinum analogue carboplatin to induce an accumulation of interstrand cross-links in glioma cells, leading to cytotoxicity.

Except for some reports in melanoma [42] and glioblastoma [6] not much is known about deregulation of non-mutated Fanconi proteins in cancer. The Fanconi core component FANCD2 seems primarily overexpressed in more aggressively growing gliomas, and protein expression has been shown to correlate with glioma grade [6]. This observation is in line with our gene expression analysis, where we find strong *FANCD2* upregulation in HGGs compared to healthy brain tissues. Also protein expression analysis showed FANCD2 overexpression in all our FANCD2 wildtype pHGG cell models compared to astrocytes *in vitro*, independent of their molecular background or treatment history. This overexpression seems specific for FANCD2, as we did not find other Fanconi complex genes overexpressed to the same extent in glioma gene expression datasets compared to healthy brain tissues. This may indicate that FANCD2 plays a vital role in HGGs that is distinct from the traditional Fanconi repair machinery, which relies on Fanconi core complex formation [43,44].

In our *in vitro* pHGG models we observed that celastrol affects glioma cell viability at lower concentrations than described in literature for other cancer cell types [45]. This could be explained by the relatively quick proliferation speed and higher mutational burden of

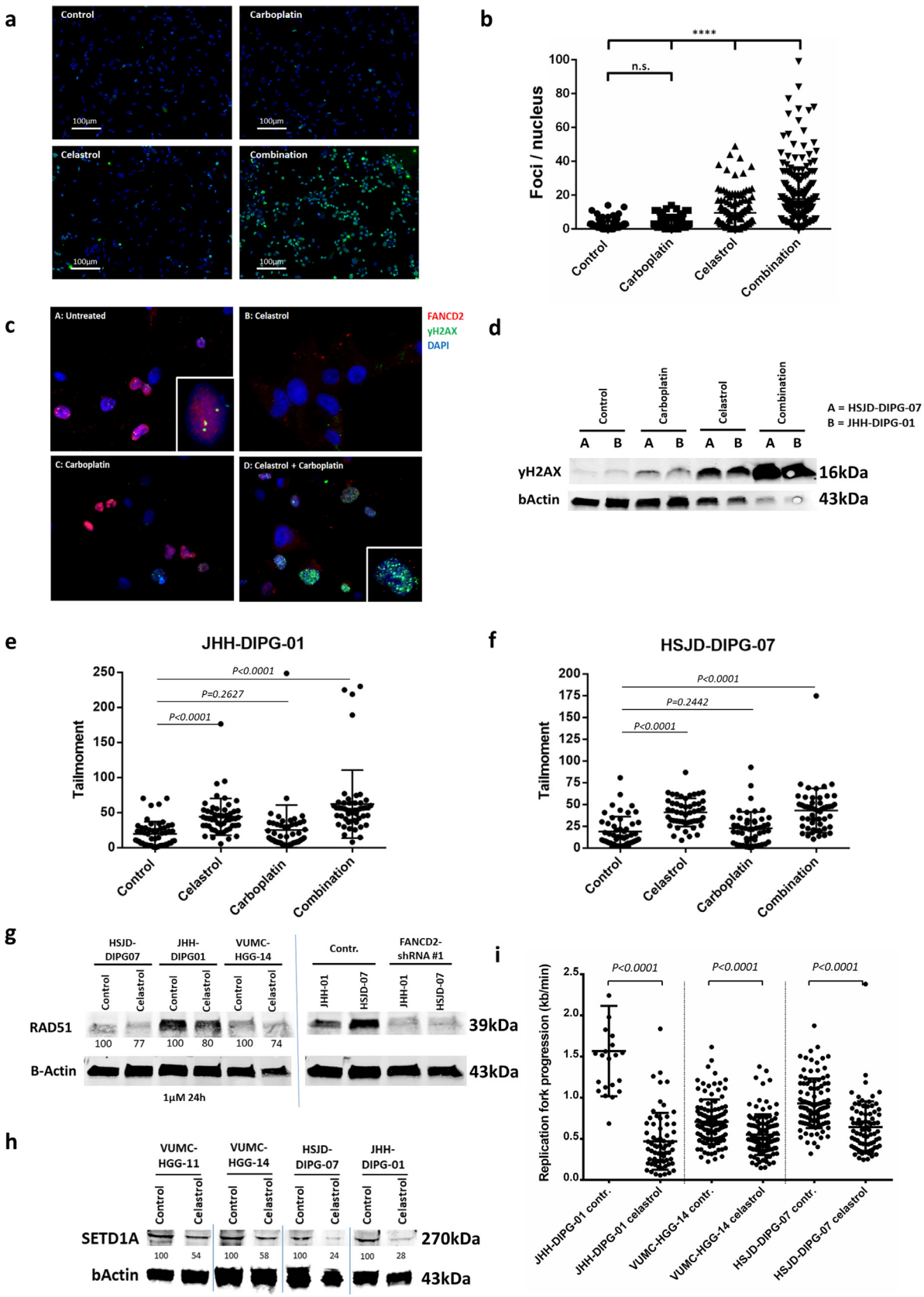

Fig. 5. Celastrol treatment impairs DNA-damage repair and stalls replication forks.

(a) γH2AX immunofluorescent stainings in VUMC-HGG-09 cells after drug treatment (celastrol 1 μM, carboplatin 3 μM) (24 h). γH2AX is depicted in green and DAPI in blue.

(b) Quantification of yH2AX foci per nuclei in VUMC-HGG-09 cells after drug treatment (celastrol 1 μM, carboplatin 3 μM) (24 h). *P*-values between each group are <0.0001, except for control *vs*. carboplatin ($P = 0{,}08981$).

(c) Immunofluorescent stainings of VUMC-HGG-09 cells after drug treatment (24 h). (a): untreated; (b): celastrol 1 μM; (c): carboplatin 3 μM; (d): combination. FANCD2 staining is depicted in magenta, yH2AX in green, and DAPI in blue.

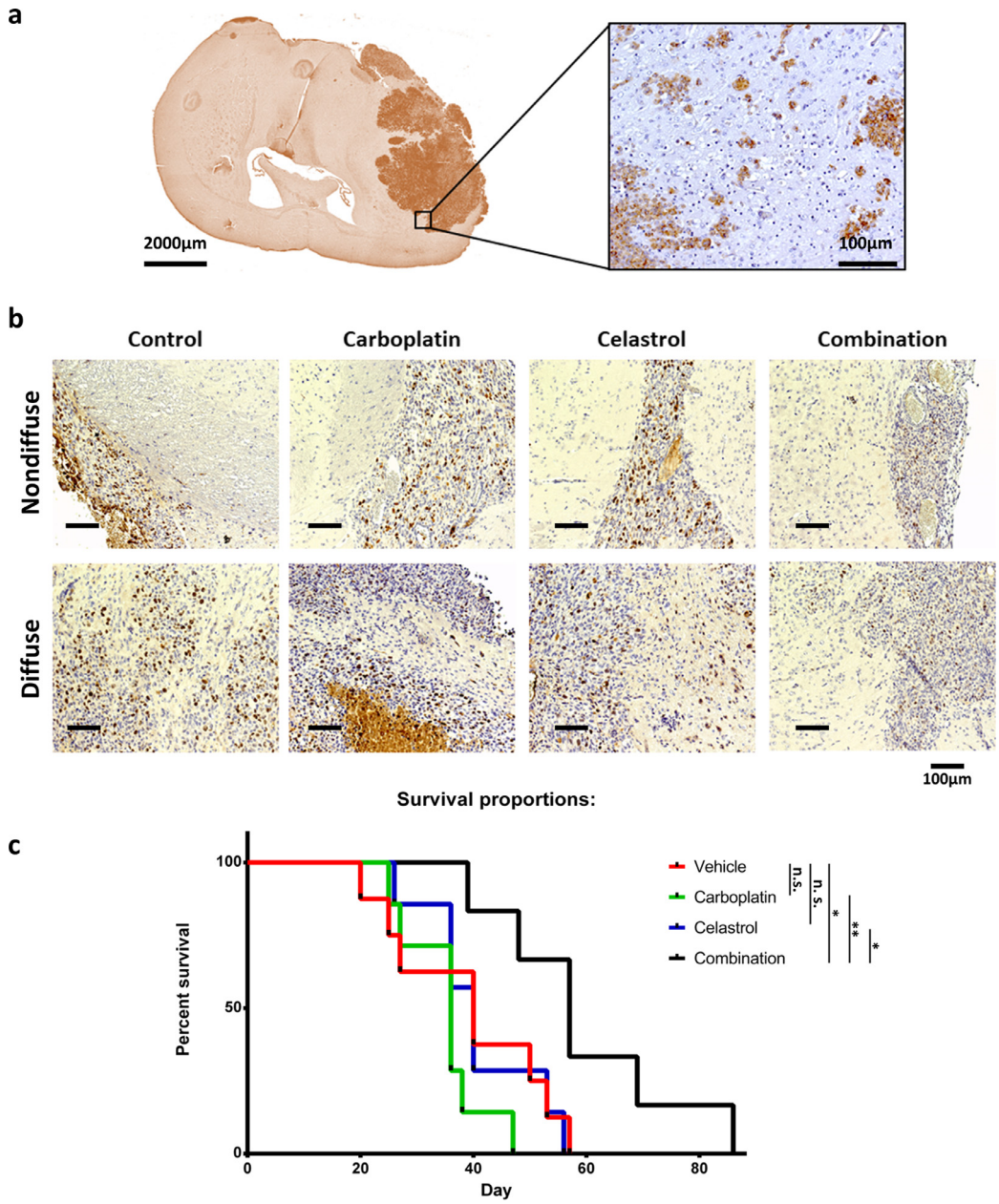

Fig. 6. Celastrol and carboplatin combination therapy prolongs survival in a patient-derived pediatric glioblastoma xenograft model *in vivo*.

(a) Immunohistochemical staining of human vimentin (brown) in the brain of a VUMC-HGG-14 xenograft-bearing mouse, revealing a diffuse growth pattern typical of GBM. One representative brain slide is shown.

(b) Survival analysis of VUMC-HGG-14 orthotopic xenograft-bearing mice treated with vehicle (red line, $n = 8$), celastrol (blue line, $n = 7$), carboplatin (green line, $n = 7$) or a combination of both (black line, $n = 6$). The combination treated group shows significant benefit over the other 3 groups. *: $P < 0.05$, **: $P < 0.005$ (log-rank test) ($n = 28$).

(c) Human KI-67 immunohistochemical staining (in brown) in VUMC—HGG-14 tumor areas in the brains of each mouse group. Edges of diffuse and nondiffuse areas are shown. (For interpretation of the references to color in this figure legend, the reader is referred to the web version of this article.)

(d) Western blot showing γH2AX in HSJD-DIPG-07 and JHH-DIPG-01 at 24 h after treatment with either carboplatin, celastrol or a combination thereof. Protein loading was lowered in celastrol and combination treated conditions to correct for γH2AX overexposure.

(e) Dot plot representing tail length of individual JHH-DIPG-01 cells after 24 h of treatment with celastrol, carboplatin or a combination thereof, as determined by neutral comet assay. At least 50 tail lengths per condition are represented.

(f) Dot plot representing tail length of individual HSJD-DIPG-07 cells after 24 h of treatment with celastrol, carboplatin or a combination thereof, as determined by neutral comet assay. At least 50 tail lengths per condition are represented.

(g) Left column: western blot showing depletion of RAD51 after celastrol (1 μM) treatment for 24 h. Intensity of the signal was analyzed using ImageJ and corrected for β-actin expression. Right column: western blot showing depletion of RAD51 in wildtype cells *vs.* FANCD2 knockdown cells.

(h) Western blot showing depletion of SETD1A after celastrol (1 μM) treatment for 24 h. Intensity of the signal was analyzed using ImageJ and corrected for β-actin expression.

(i) Dot plot representing replication fork progression in kb/min in three pHGG models with and without 1 μM celastrol treatment for 24 h, as determined by DNA fiber assay.

All P-values of Fig. 4 were determined using the Mann–Whitney U test. (For interpretation of the references to color in this figure legend, the reader is referred to the web version of this article.)

HGGs compared to lower-grade tumors [46], through which HGGs might rely on higher FANCD2 expression levels for their replication errors to be restored. Furthermore, we show that celastrol effectively downregulates FANCD2 protein expression in a post-transcriptional manner, without leading to a complete loss of FANCD2 protein. This likely explains why celastrol treatment is so well tolerated *in vivo*, as healthy cells remain viable under low FANCD2 expression levels [47].

In order to confirm that celastrol causes FANCD2-mediated fork degradation, we used RAD51 and SETD1A as markers for this process. RAD51 has a central role in DNA-repair by promoting homologous recombination repair and acts as a facilitator for the formation of reversed replication forks, where it protects nascent DNA strands from nuclease digestion [48]. Recent literature describes a direct link between FANCD2 and RAD51, via modification of histone methylation [39]. FANCD2 recruits histone chaperones that modulate histone mobilization, allowing for SETD1A mediated mono-methylation to occur at the histone 3 lysine 4 (H3K4) site. H3K4 mono-methylation is vital for histone accessibility onto the regressed arms of reversed forks, which stabilises RAD51 filaments at the 3′ end of nascent DNA. Since RAD51 prevents digestion of this nascent DNA by stabilizing it, RAD51 acts as a guardian against uncontrolled DNA resection. It is therefore hypothesised that post-transcriptional depletion of FANCD2 causes loss of RAD51 protein expression via lost H3K4 mono-methylation, which is the result of lost SETD1A protein. We therefore consider the loss of SETD1A and RAD51 as markers for increased genomic instability. Correspondingly, using the DNA-fiber assay we were able to confirm that celastrol treatment induces stalled replication forks, which contributes to genomic instability.

Even though DNA-crosslinking, in contrast to DSB formation, seems the essential mechanism to achieve pHGG-specific cell death after celastrol treatment, we used γH2AX as a marker for DNA-damage. γH2AX is a widely used marker for DNA-DSBs or G2/M arrest [38,49]. However, DSBs are also the long term result of non-repaired DNA-crosslinks. Where γH2AX expression peaks seconds after induction of direct DSBs via irradiation, γH2AX levels peak 12 to 24 h after the addition of DNA-crosslinking agents [50]. When intracellular repair machineries fail to repair these interstrand crosslinks, degradation of DNA occurs and DSBs arise [51]. Furthermore, next to being a marker for DNA DSBs, γH2AX has been shown to be a marker for stalled replication forks [52]. Therefore, the γH2AX foci increase between celastrol *versus* combination treatment, while no increase in DSB between these groups is observed, could be the result of interstrand-crosslink accumulation as a cause of stalled replication forks. These findings were further confirmed when we found no synergism between celastrol and topotecan, which is, like carboplatin, another clinically relevant DNA-damaging agent but without any interstrand-crosslink abilities.

In our study we used celastrol treatment to induce FANCD2 degradation. Celastrol is a natural plant-derivative that crosses the BBB and was found to have several physiological properties, including strong anti-inflammatory and antioxidant activities [53,54]. As celastrol treatment did not cause any adverse effects *in vivo* and has been used safely in traditional eastern medicine for centuries, we argue that celastrol (or equivalent derivatives) holds great promise for clinical use in HGG patients. Importantly, a synthetic celastrol analogue (ERX-1000, ERX Pharmaceuticals LLC. Brooklyn, NY, USA) is currently being produced for clinical studies, albeit for other indications, which could contribute to the translational potential of FANCD2 inhibition in the clinic. Carboplatin, which is less toxic than cisplatin and crosses the BBB, has been used in patients for decades and the step to using this compound in HGG patients is highly feasible [10,55].

In vivo experiments using a glioblastoma orthotopic xenograft model showed a significant survival benefit for mice treated with celastrol and carboplatin combination therapy over monotherapy and non-treated groups. This correlated with a reduced expression of the proliferation marker Ki-67 in the combination therapy group, while no changes of cleaved caspase-3 were observed in both healthy and malignant tissues. While this pledges for an absence of treatment-induced neurotoxicity, care needs to be taken, as the brains used for these stainings were collected from the first dropout mice of each group, three weeks after treatment. This is a limitation of the study and future studies should histologically examine brain tissues during the treatment procedure, in order to show the direct effect of treatment on Ki-67 and cleaved caspase-3. Interestingly, we observed less, and later, severe neurological symptoms in the group treated with both celastrol and carboplatin, albeit as a non-significant trend. BLI imaging of tumor growth was stopped after 41 days due to the diffuse growth characteristics of the tumors, which affected the observed BLI signal based on its migration pattern. However, the results from this first *in vivo* trial, combined with our *in vitro* data, could serve as the basis for more in depth studies into the efficacy of celastrol and carboplatin combination therapy in molecularly different HGG models *in vivo*. Especially a more thorough *in vivo* investigation in H3.1K27 and H3.3K27 mutated DIPG models would be a valuable addition to the findings presented here.

In conclusion, we demonstrate that FANCD2 plays a vital role in maintaining genomic integrity in pHGG cells and that degradation of FANCD2 via celastrol treatment sensitizes HGGs to carboplatin-mediated DNA damage. Our study demonstrates that FANCD2 knockdown in HGGs causes stalled replication forks which disables the tumor cells to unwind DNA-crosslinks. Since HGGs are highly proliferative and depend on fork-mediated DNA-repair mechanisms, we propose FANCD2 as a novel candidate for therapeutic intervention in HGGs.

Funding sources

This study was funded by a grant from the Children Cancer-Free Foundation (KIKA, project 210). The disclosed funders had no role in study design, data collection and analysis, decision to publish, or preparation of the manuscript.

Declaration of Competing Interest

D.S.M reports grants from the Children Cancer-Free Foundation (KIKA, project 210), during the conduct of the study. None of the other authors declare any conflicts of interest.

CRediT authorship contribution statement

Dennis S. Metselaar: Conceptualization, Methodology, Investigation, Data curation, Formal analysis, Validation, Visualization, Writing - original draft, Writing - review & editing. **Michaël H. Meel:** Conceptualization, Methodology, Writing - original draft. **Bente Benedict:** Investigation, Methodology, Writing - original draft. **Piotr Waranecki:** Investigation, Writing - original draft. **Jan Koster:** Formal analysis, Software, Writing - original draft. **Gertjan J.L. Kaspers:** Writing - original draft, Supervision. **Esther Hulleman:** Writing - original draft, Supervision, Conceptualization, Funding acquisition.

Supplementary materials

Supplementary material associated with this article can be found in the online version at doi:10.1016/j.ebiom.2019.10.062.

References

[1] Pagano G, d'Ischia M, Pallardo FV. Fanconi anemia (FA) and crosslinker sensitivity: *re*-appraising the origins of FA definition. Pediatr Blood Cancer 2015;62(7):1137–43.
[2] Su X, Huang J. The fanconi anemia pathway and dna interstrand cross-link repair. Protein Cell 2011;2(9):704–11.
[3] Niedernhofer LJ, Lalai AS, Hoeijmakers JH. Fanconi anemia (cross)linked to dna repair. Cell 2005;123(7):1191–8.

[4] Walden H, Deans AJ. The fanconi anemia dna repair pathway: structural and functional insights into a complex disorder. Ann Rev Biophys 2014;43:257–78.
[5] Liang CC, Li ZL, Lopez-Martinez D, Nicholson WV, Venien-Bryan C, Cohn MA. The FANCD2-FANCI complex is recruited to DNA interstrand crosslinks before monoubiquitination of FANCD2. Nat Commun 2016;7.
[6] Patil AA, Sayal P, Depondt ML, Beveridge RD, Roylance A, Kriplani DH, et al. FANCD2 re-expression is associated with glioma grade and chemical inhibition of the fanconi anaemia pathway sensitises gliomas to chemotherapeutic agents. Oncotarget 2014;5(15):6414–24.
[7] Paris D, Ganey NJ, Laporte V, Patel NS, Beaulieu-Abdelahad D, Bachmeier C, et al. Reduction of beta-amyloid pathology by celastrol in a transgenic mouse model of Alzheimer's disease. J Neuroinflammation 2010;7:17.
[8] Wang GZ, Liu YQ, Cheng X, Zhou GB. Celastrol induces proteasomal degradation of FANCD2 to sensitize lung cancer cells to DNA crosslinking agents. Cancer Sci 2015;106(7):902–8.
[9] Screnci D, McKeage MJ. Platinum neurotoxicity: clinical profiles, experimental models and neuroprotective approaches. J Inorg Biochem 1999;77(1–2):105–10.
[10] Newton HB, Slivka MA, Volpi C, Bourekas EC, Christoforidis GA, Baujan MA, et al. Intra-arterial carboplatin and intravenous etoposide for the treatment of metastatic brain tumors. J Neurooncol 2003;61(1):35–44.
[11] Jansen MH, Lagerweij T, Sewing AC, Vugts DJ, van Vuurden DG, Molthoff CF, et al. Bevacizumab Targeting Diffuse Intrinsic Pontine Glioma: results of 89Zr-Bevacizumab Pet Imaging In Brain Tumor Models. Mol Cancer Ther 2016;15(9):2166–74.
[12] Taylor IC, Hutt-Cabezas M, Brandt WD, Kambhampati M, Nazarian J, Chang HT, et al. Disrupting notch slows diffuse intrinsic pontine glioma growth, enhances radiation sensitivity, and shows combinatorial efficacy with bromodomain inhibition. J Neuropath Exp Neur 2015;74(8):778–90.
[13] Grasso CS, Tang Y, Truffaux N, Berlow NE, Liu L, Debily MA, et al. Functionally defined therapeutic targets in diffuse intrinsic pontine glioma. Nat Med 2015;21(6):555–9.
[14] Nagaraja S, Vitanza NA, Woo PJ, Taylor KR, Liu F, Zhang L, et al. Transcriptional dependencies in diffuse intrinsic pontine glioma. Cancer Cell 2017;31(5):635–52 .e6.
[15] Meel MH, de Gooijer MC, Guillen Navarro M, Waranecki P, Breur M, Buil LCM, et al. MELK inhibition in diffuse intrinsic pontine glioma. Clin Cancer Res 2018;24(22):5645–57.
[16] Veringa SJ, Biesmans D, van Vuurden DG, Jansen MH, Wedekind LE, Horsman I, et al. *In vitro* drug response and efflux transporters associated with drug resistance in pediatric high grade glioma and diffuse intrinsic pontine glioma. PLoS ONE 2013;8(4):e61512.
[17] Meel MH, Metselaar DS, Waranecki P, Kaspers GJL, Hulleman E. An efficient method for the transduction of primary pediatric glioma neurospheres. MethodsX 2018;5:173–83.
[18] Meel MH, Sewing ACP, Waranecki P, Metselaar DS, Wedekind LE, Koster J, et al. Culture methods of diffuse intrinsic pontine glioma cells determine response to targeted therapies. Exp Cell Res 2017;360(2):397–403.
[19] Berchtold NC, Cribbs DH, Coleman PD, Rogers J, Head E, Kim R, et al. Gene expression changes in the course of normal brain aging are sexually dimorphic. Proc Natl Acad Sci U S A 2008;105(40):15605–10.
[20] Harris LW, Lockstone HE, Khaitovich P, Weickert CS, Webster MJ, Bahn S. Gene expression in the prefrontal cortex during adolescence: implications for the onset of schizophrenia. BMC Med Genom 2009;2:28.
[21] Roth RB, Hevezi P, Lee J, Willhite D, Lechner SM, Foster AC, et al. Gene expression analyses reveal molecular relationships among 20 regions of the human CNS. Neurogenetics 2006;7(2):67–80.
[22] Gravendeel LA, Kouwenhoven MC, Gevaert O, de Rooi JJ, Stubbs AP, Duijm JE, et al. Intrinsic gene expression profiles of gliomas are a better predictor of survival than histology. Cancer Res 2009;69(23):9065–72.
[23] Sun L, Hui AM, Su Q, Vortmeyer A, Kotliarov Y, Pastorino S, et al. Neuronal and glioma-derived stem cell factor induces angiogenesis within the brain. Cancer Cell 2006;9(4):287–300.
[24] Murat A, Migliavacca E, Gorlia T, Lambiv WL, Shay T, Hamou MF, et al. Stem cell-related "self-renewal" signature and high epidermal growth factor receptor expression associated with resistance to concomitant chemoradiotherapy in glioblastoma. J Clin Oncol: Off J Am Soc Clin Oncol 2008;26(18):3015–24.
[25] Paugh BS, Qu C, Jones C, Liu Z, Adamowicz-Brice M, Zhang J, et al. Integrated molecular genetic profiling of pediatric high-grade gliomas reveals key differences with the adult disease. J Clin Oncol: Off J Am Soc Clin Oncol 2010;28(18):3061–8.
[26] Paugh BS, Broniscer A, Qu C, Miller CP, Zhang J, Tatevossian RG, et al. Genome-wide analyses identify recurrent amplifications of receptor tyrosine kinases and cell-cycle regulatory genes in diffuse intrinsic pontine glioma. J Clin Oncol: Off J Am Soc Clin Oncol 2011;29(30):3999–4006.
[27] Kawaguchi A, Yajima N, Tsuchiya N, Homma J, Sano M, Natsumeda M, et al. Gene expression signature-based prognostic risk score in patients with glioblastoma. Cancer Sci 2013;104(9):1205–10.
[28] Hall MD, Telma KA, Chang KE, Lee TD, Madigan JP, Lloyd JR, et al. Say no to DMSO: dimethylsulfoxide inactivates cisplatin, carboplatin, and other platinum complexes. Cancer Res 2014;74(14):3913–22.
[29] Olive PL, Banath JP. The comet assay: a method to measure dna damage in individual cells. Nat Protoc 2006;1(1):23–9.
[30] Benedict B, van Harn T, Dekker M, Hermsen S, Kucukosmanoglu A, Pieters W, et al. Loss of p53 suppresses replication-stress-induced dna breakage in G1/S checkpoint deficient cells. Elife 2018;7.
[31] Jackson DA, Pombo A. Replicon clusters are stable units of chromosome structure: evidence that nuclear organization contributes to the efficient activation and propagation of s phase in human cells. J Cell Biol 1998;140(6):1285–95.
[32] van Hennik MB, van der Vijgh WJ, Klein I, Elferink F, Vermorken JB, Winograd B, et al. Comparative pharmacokinetics of cisplatin and three analogues in mice and humans. Cancer Res 1987;47(23):6297–301.
[33] Liu JL, Lee J, Hernandez MAS, Mazitschek R, Ozcan U. Treatment of obesity with celastrol. Cell 2015;161(5):999–1011.
[34] Ianevski A, He L, Aittokallio T, Tang J. SynergyFinder: a web application for analyzing drug combination dose-response matrix data. Bioinformatics 2017;33(15):2413–5.
[35] Yadav B, Wennerberg K, Aittokallio T, Tang J. Searching for drug synergy in complex dose-response landscapes using an interaction potency model. Comput Struct Biotechnol J 2015;13:504–13.
[36] Hayashi M, Saito Y, Kawashima S. Calpain activation is essential for membrane fusion of erythrocytes in the presence of exogenous Ca2+. Biochem Biophys Res Commun 1992;182(2):939–46.
[37] Kaiser MG, Parsa AT, Fine RL, Hall JS, Chakrabarti I, Bruce JN. Tissue distribution and antitumor activity of topotecan delivered by intracerebral clysis in a rat glioma model. Neurosurgery 2000;47(6):1391–8 discussion 8-9.
[38] Kuo LJ, Yang LX. Gamma-H2AX - a novel biomarker for dna double-strand breaks. In Vivo (Brooklyn) 2008;22(3):305–9.
[39] Higgs MR, Sato K, Reynolds JJ, Begum S, Bayley R, Goula A, et al. Histone methylation by setd1a protects nascent DNA through the nucleosome chaperone activity of FANCD2. Mol Cell 2018;71(1):25.
[40] Bhat KP, Krishnamoorthy A, Dungrawala H, Garcin EB, Modesti M, Cortez D. RADX modulates RAD51 activity to control replication fork protection. Cell Rep 2018;24(3):538–45.
[41] Baumann BC, Dorsey JF, Benci JL, Joh DY, Kao GD. Stereotactic intracranial implantation and *in vivo* bioluminescent imaging of tumor xenografts in a mouse model system of glioblastoma multiforme. J Vis Exp 2012(67).
[42] Kao WH, Riker AI, Kushwaha DS, Ng K, Enkemann SA, Jove R, et al. Upregulation of Fanconi anemia DNA repair genes in melanoma compared with non-melanoma skin cancer. J Invest Dermatol 2011;131(10):2139–42.
[43] Yamamoto K, Nihrane A, Aglipay J, Sironi J, Arkin S, Lipton JM, et al. Upregulated ATM gene expression and activated DNA crosslink-induced damage response checkpoint in fanconi anemia: implications for carcinogenesis. Mol Med 2008;14(3–4):167–74.
[44] Huang Y, Leung JW, Lowery M, Matsushita N, Wang Y, Shen X, et al. Modularized functions of the Fanconi anemia core complex. Cell Rep 2014;7(6):1849–57.
[45] Yang H, Chen D, Cui QC, Yuan X, Dou QP. Celastrol, a triterpene extracted from the Chinese "Thunder of god vine," is a potent proteasome inhibitor and suppresses human prostate cancer growth in nude mice. Cancer Res 2006;66(9):4758–65.
[46] Johnson A, Severson E, Gay L, Vergilio JA, Elvin J, Suh J, et al. Comprehensive genomic profiling of 282 pediatric Low- and High-Grade gliomas reveals genomic drivers, tumor mutational burden, and hypermutation signatures. Oncologist 2017;22(12):1478–90.
[47] Lu WT, Lemonidis K, Drayton RM, Nouspikel T. The Fanconi anemia pathway is downregulated upon macrophage differentiation through two distinct mechanisms. Cell Cycle 2011;10(19):3300–10.
[48] Schlacher K, Wu H, Jasin M. A distinct replication fork protection pathway connects Fanconi anemia tumor suppressors to RAD51-BRCA1/2. Cancer Cell 2012;22(1):106–16.
[49] Tu WZ, Li B, Huang B, Wang Y, Liu XD, Guan H, et al. gammaH2AX foci formation in the absence of dna damage: mitotic H2AX phosphorylation is mediated by the DNA-PKcs/CHK2 pathway. FEBS Lett 2013;587(21):3437–43.
[50] Clingen PH, Wu JY, Miller J, Mistry N, Chin F, Wynne P, et al. Histone H2AX phosphorylation as a molecular pharmacological marker for dna interstrand crosslink cancer chemotherapy. Biochem Pharmacol 2008;76(1):19–27.
[51] Wu J, Clingen PH, Spanswick VJ, Mellinas-Gomez M, Meyer T, Puzanov I, et al. gamma-H2AX foci formation as a pharmacodynamic marker of DNA damage produced by DNA cross-linking agents: results from 2 phase I clinical trials of SJG-136 (SG2000). Clin Cancer Res. 2013;19(3):721–30.
[52] Sirbu BM, Couch FB, Feigerle JT, Bhaskara S, Hiebert SW, Cortez D. Analysis of protein dynamics at active, stalled, and collapsed replication forks. Genes Dev 2011;25(12):1320–7.
[53] Allison AC, Cacabelos R, Lombardi VR, Alvarez XA, Vigo C. Celastrol, a potent antioxidant and anti-inflammatory drug, as a possible treatment for Alzheimer's disease. Prog Neuropsychopharmacol Biol Psychiatry 2001;25(7):1341–57.
[54] Venkatesha SH, Dudics S, Astry B, Moudgil KD. Control of autoimmune inflammation by celastrol, a natural triterpenoid. Pathog Dis 2016;74(6).
[55] Murray LJ, Bridgewater CH, Levy D. Carboplatin chemotherapy in patients with recurrent high-grade glioma. Clin Oncol (R Coll Radiol) 2011;23(1):55–61.